

AcpM, the Meromycolate Extension Acyl Carrier Protein of *Mycobacterium tuberculosis*, Is Activated by the 4'-Phosphopantetheinyl Transferase PptT, a Potential Target of the Multistep Mycolic Acid Biosynthesis

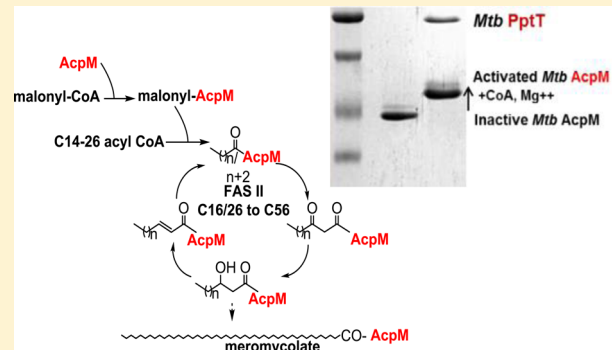
Oren Zimhony,^{*,†,||} Alon Schwarz,^{‡,§,||} Maria Raitses-Gurevich,[‡] Yoav Peleg,[⊥] Orly Dym,[⊥] Shira Albeck,[⊥] Yigal Burstein,[§] and Zippora Shakhd[‡]

[†]Kaplan Medical Center, Affiliated to the School of Medicine, Hebrew University of Jerusalem and Hadassah Medical Center, POB1 Rehovot 76100, Israel

[‡]Department of Structural Biology, [⊥]Israel Structural Proteomics Center, and [§]Department of Organic Chemistry, Weizmann Institute of Science, 234 Herzl Street, Rehovot 7610001, Israel

S Supporting Information

ABSTRACT: Modification of acyl carrier proteins (ACP) or domains by the covalent binding of a 4'-phosphopantetheine (4'-PP) moiety is a fundamental condition for activation of fatty acid synthases (FASes) and polyketide synthases (PKSes). Binding of 4'-PP is mediated by 4' phosphopantetheinyl transferases (PPTases). *Mycobacterium tuberculosis* (*Mtb*) possesses two essential PPTases: acyl carrier protein synthase (*Mtb* AcpS), which activates the multidomain fatty acid synthase I (FAS I), and *Mtb* PptT, an Sfp-type broad spectrum PPTase that activates PKSes. To date, it has not been determined which of the two *Mtb* PPTases, AcpS or PptT, activates the meromycolate extension ACP, *Mtb* AcpM, en route to the production of mycolic acids, the main components of the mycobacterial cell wall. In this study, we tested the enzymatic activation of a highly purified *Mtb* apo-AcpM to *Mtb* holo-AcpM by either *Mtb* PptT or *Mtb* AcpS. By using SDS-PAGE band shift assay and mass spectrometry analysis, we found that *Mtb* PptT is the PPTase that activates *Mtb* AcpM. We measured the catalytic activity of *Mtb* PptT toward CoA, using an activation assay of a blue pigment synthase, BpsA (a nonribosomal peptide synthase, NRPS). BpsA activation by *Mtb* PptT was inhibited by *Mtb* apo-AcpM through competition for CoA, in accord with *Mtb* AcpM activation. A structural model of the putative interaction between *Mtb* PptT and *Mtb* AcpM suggests that both hydrophobic and electrostatic interactions stabilize this complex. To conclude, activation of *Mtb* AcpM by *Mtb* PptT reveals a potential target of the multistep mycolic acid biosynthesis.



Multidrug-resistant tuberculosis arises as a result of an inappropriate usage and interruption of the relatively long and complex drug regimen required for lasting cure.

The therapeutic options for multidrug-resistant strains of *Mycobacterium tuberculosis* (*Mtb*) are scarce.¹ Thus, there is a need for target identification followed by new drug development to simplify and shorten therapy, and to prevent the emergence of resistance while providing additional options for treating drug-resistant tuberculosis. *Mtb* possesses a unique lipid-rich cell wall that confers virulence, persistence, and drug resistance, which is comprised mainly of α -alkyl- β -hydroxyl C80-90 fatty acids termed mycolic acids, and several polyketides.²⁻⁵ Several steps in mycolic acid biosynthesis were identified as drug targets for first-line antituberculosis agents.⁶ Mycobacteria uniquely between bacteria possess two types of fatty acid synthase systems, FAS I and FAS II and 18 polyketide synthases (PKSes).^{5,6} FAS I is a multifunctional, multidomain protein that elongates acyl-CoA to C16:0–26:0

fatty acids.^{7,8} FAS II elongates C16:0–26:0 to C56:0 meromycolate, which may undergo various modifications, and is finally condensed with C26:0 to mycolic acid by PKS13.^{6,9,10} The acyl intermediates produced during these processes are attached covalently to an acyl carrier protein (ACP) domain of FAS I or PKS, or to a discrete meromycolate extension ACP of FAS II system, designated *Mtb* AcpM.^{6,11} FAS and PKSes are activated through the transfer of a 4'-phosphopantetheine (4'-PP) group from CoA to an ACP, a reaction that is catalyzed by a 4'-PP transferase (PPTase) enzyme.

The PPTases have been classified based on sequence and structural features, into three classes.^{12,13} The first class includes the ACP synthetases, AcpS-type PPTases, which contain

Received: November 21, 2014

Revised: March 6, 2015

Published: March 18, 2015

approximately 120 amino acid residues arranged in an α/β fold and which function as a homotrimer.¹⁴ The AcpS-type PPTases primarily activate only ACPs of FAS I or FAS II systems. The second class includes Sfp-type PPTases referred to as surfactin synthetase (a *Bacillus subtilis* PPTase activating enzyme). These are monomers of about 240 residues whose structure displays two domains, related to each other by a pseudo 2-fold symmetry. Each domain has a homologous structure to a single monomer of the trimeric AcpS-type PPTase. The active site is situated in a cleft formed by the two domains.^{12,15,16} The Sfp-type PPTases activate the ACPs and peptidyl carrier (PCPs) domains for secondary metabolism, such as nonribosomal peptide synthases (NRPS) and polyketide synthases (PKSes). They often exhibit a broad acceptor substrate specificity compared to the AcpS-type PPTases.¹⁷ The third member of the PPTase family is an AcpS-like domain that activates the ACP domain of the α subunit of yeast FAS I complex.^{18–20}

Two genes encoding PPTases, *acpS* (*Rv2523*) and *pptT* (*Rv2794*), were identified in *Mtb* genome and shown to be essential for mycobacterium viability.²¹ *pptT* was recently shown to be required for growth and persistence of *Mtb* in murine macrophages and in a mouse model of tuberculosis, supporting its potential as a drug target.^{21,22} The AcpSes of mycobacteria and corynebacteria were both shown to activate FAS I.²³ *Mtb* PptT, the Sfp-type broad spectrum PPTase, was first found to be an activator of NRPS *MtbB* and *MtbE*, producing the sidereophore mycobactin²⁴ and subsequently was shown to activate type-I PKS including PKS13.^{21,22}

Mtb AcpM, the meromycolate extension ACP for the *Mtb* FAS II enzymes, was presumed to be activated by *Mtb* AcpS, the FAS I activator.²¹ This assumption was based on extrapolation from the data on most other bacterial species that possess a FAS II system, in which ACPs are usually activated by AcpSes.²¹ Expression of *Mtb* AcpM in *Escherichia coli* yields, in addition to the apo-form, holo and acylated *Mtb* AcpM that result from the endogenous *E. coli* AcpS activity on *Mtb* AcpM *in vivo* and *in vitro*.^{25,26} The conversion of *Mtb* apo-AcpM to holo-AcpM by *E. coli* AcpS can be explained by the structural and sequence homology of *Mtb* AcpM to the *E. coli* ACP (as well as other FAS II ACPs). In all ACP proteins, the active serine which binds 4'-PP is within a conserved DSL motif (Asp, Ser, Leu), and there is a high degree of structural homology between ACPs and *Mtb* AcpM in the region adjacent to this motif.^{11,27} For *Mtb* AcpM the activated serine was suggested to be in position 41.¹¹ *Mtb* AcpM activation by *Mtb* AcpS has been suggested by a study showing an incorporation of fluorescently labeled 4'-PP into *Mtb* AcpM in the presence of *Mtb* AcpS.²⁸

Whereas *Mtb* AcpM structure displays a close similarity to other ACPs, the proposed activator *Mtb* AcpS differs from other AcpSes.²⁷ Analysis of the X-ray structure of the complex of ACP with AcpS from *B. subtilis* demonstrated an electrostatic complementarity between an electropositive surface of *B. subtilis* AcpS and electronegative surface of *B. subtilis* ACP, which facilitates the interaction between the two.¹⁴ However, the crystal structure of *Mtb* AcpS revealed a moderately electronegative surface instead of the electropositive surface common to AcpSes from other species.²⁷

Here we present an *in vitro* study aimed to resolve and characterize the PPTase activator of *Mtb* AcpM. We studied the formation of *Mtb* holo-AcpM from a highly purified *Mtb* apo-AcpM in the presence of either *Mtb* AcpS or *Mtb* PptT. We showed for the first time that *Mtb* PptT activates *Mtb* AcpM,

whereas *Mtb* AcpS does not. Catalytic activity and binding studies as well as a model of the interaction between *Mtb* PptT and *Mtb* AcpM based on the recent structure of *Mtb* PptT²⁹ were used to support these findings.

EXPERIMENTAL PROCEDURES

Cloning of *Mtb* PPTases and AcpM (Primers Are Listed in Supplementary Table 1, Supporting Information).

Rv2794 gene encoding *Mtb* PptT was PCR amplified from *Mycobacterium bovis* (BCG) genomic library³⁰ using the primers in Supplementary Table 1. *Mtb* PptT was cloned into the *Bam*H I and *Sac*I sites at the first expression cassette of the vector pACYCDuet-1 (Novagen) fused to a 6X His tag at the N-terminus. The *Mtb* *acpM* (*Rv2244*) gene was amplified from a genomic library of H37Rv and cloned into the expression vector, pET21-TevH, fused to 6X His at the N-terminus using a restriction free (RF) procedure^{31,32} with primers listed in Supplementary Table 1. The pET21-*acpM* plasmid was subjected to site directed mutagenesis using QuickChange XL Stratagene for the replacement of Ser41 by alanine using two overlapping mutagenic primers that are listed in Supplementary Table 1. *Mtb* *acpS* was cloned as described previously.²⁷

Cloning of *Corynebacterium striatum* (ATCC-6940) PptCS.

The gene *pptCS* (PptCS NCBI reference sequence WP_005528976.1) was amplified from genomic DNA of *C. striatum* (ATCC-6940) and cloned into the expression vector pET28-TevH fused to 6X His at the N'-terminus using a restriction free (RF) procedure using primers listed in Supplementary Table 1. All cloned genes were sequenced to verify authenticity of the constructs.

Protein Expression. *Mtb* AcpM, *Mtb* PptT, and *C. striatum* PptCS were expressed in *E. coli* strain BL21 (DE3) as N-terminal His fusion proteins. In addition, *Mtb* AcpM was expressed in BL21 (DE3) in which the endogenous Sfp-like PPTase, EntD (BL21(DE3) Δ EntD), was deleted through the TargeTron procedure (Sigma-Aldrich). For both PPTases and *Mtb* AcpM, the following protocol was employed. Cells were grown to mid log phase ($OD_{600} = 0.6$) in 2YT media and induced by 200 μ M isopropyl β -D-1-thiogalactopyranoside (IPTG) and 0.2% (w/v) lactose. Cells were shaken at 37 °C for another 3 h and harvested by centrifugation, washed once (20 mM Tris, pH 8.1, 150 mM NaCl), and kept at –80 °C for further use. *Mtb* AcpS was expressed as described previously.²⁷

Protein Purification. *Mtb* PptT. *Mtb* PptT is poorly soluble as described in previous studies.^{22,24} L-Arg was added to the purification protocol to stabilize the protein.³³ *Mtb* PptT purification was performed at 4 °C. Cells were suspended in buffer A (20 mM Tris pH 8.1, 150 mM NaCl, 0.25 M L-arginine, 10% v/v glycerol, 0.012% Triton X100, and 0.3 mM DTT) to which 0.2% v/v protease inhibitor cocktail set III (Calbiochem) was added and lysed by sonication (Sonics Vibracell). The clarified supernatant was incubated with 3 mL of Ni Chelating HP resin (GE Healthcare) for about 2 h at 4 °C and loaded onto an empty column. The column was then washed twice with 5 column volumes (CV) buffer A, followed by elution with the same buffer containing 100 mM imidazole. Eluted protein was loaded onto a Superdex 200 16/60 column (GE Healthcare) equilibrated with buffer A. Fractions containing monomeric PptT (migrating at 90 mL) were pooled and kept at –80 °C for further use. *Mtb* PptT for PPTase assays was diluted to a concentration of 40 μ M in 50 mM Tris pH 8.1, 50 mM NaCl, 10 mM MgCl₂, 50 μ M CoA in 40% glycerol and

was stored at -80°C for further usage. *Mtb* AcpS was purified as described previously.²⁷

***Mtb* AcpM.** Cells were lysed as above for *Mtb* PptT. The clarified supernatant was incubated with 1 mL His Bind Fractogel resin (Novagen), equilibrated with buffer E (buffer A lacking L-arginine), for 2 h at 4°C , and loaded onto an empty column. The column was then washed four times (5 CV each) with buffer B containing PMSF and twice with buffer B containing 40 mM imidazole, followed by elution with buffer B containing 400 mM imidazole. *Mtb* AcpM was dialyzed against buffer B and concentrated yielding a mixture of *Mtb* apo- and *Mtb* holo-AcpM. Pure *Mtb* apo-AcpM was isolated from the mixture by the addition of an ion exchange step followed by gel filtration as follows. The dialyzed *Mtb* AcpM mixture was loaded onto an ion exchange column (Resource Q, GE Healthcare) equilibrated with 20 mM Tris pH 8.1 and eluted with a linear gradient to 1 M NaCl. Fractions containing *Mtb* apo-AcpM were finally separated on a Superdex 75 16/60 column (GE Healthcare). *Mtb* AcpM S41A was purified as for the native *Mtb* AcpM.

***C. striatum* PptCS.** Cells were suspended in buffer C (20 mM Tris pH 8.1, 200 mM potassium thiocyanate, 10% v/v glycerol, 0.012% Triton X100, and 0.3 mM DTT) to which 0.2% v/v protease inhibitor cocktail set III (Calbiochem) was added and lysed by sonication (Sonics Vibracell). The clarified supernatant was incubated with 3 mL of chelating HP resin (His-bind Fractogel), for about 3 h, at 4°C and packed into an empty column. The packed column was washed twice with 5 CV buffer C, and the protein was then eluted from the column with buffer F containing imidazole (0.5 M). The eluted protein was loaded onto a Superdex 200 16/60 column (GE Healthcare) equilibrated with buffer C without KSCN. Fractions containing *C. striatum* PptCS (migrating at 100 mL) were pooled and concentrated for further use.

PPTase Bioactivity Assay. Enzymatic reactions of PPTase were carried out in 20 mM Tris pH 8.1, 150 mM NaCl, 2.5 mM DTT, 500 μM coenzyme A, and 10 mM MgCl₂. *Mtb* AcpM at 50–150 μM was typically mixed with 6–8 μM of each *Mtb* AcpS, *Mtb* PptT, and Sfp synthase from *B. subtilis* (as a fusion protein with maltose binding protein, MBP, by New England Biolabs #P9302S) (MBP-Sfp^{N_EB}) in a total volume of 10–50 μL and incubated at 30°C for 2 h. Conversion of *Mtb* apo-AcpM to holo-AcpM was demonstrated by analyzing 10% (v/v) of the PPTase bioassay reaction mixture on SDS-PAGE. We used two types of SDS-PAGE on 15 or 16.5% polyacrylamide gels for optimal separation of the *Mtb* AcpM forms: tricine buffer (100 mM of Tris and tricine pH 8.3,³³ in the presence of 6 M urea, or Tris-HCl (25 mM Tris and 192 mM glycine pH 8.3). The gels were stained with Coomassie Brilliant Blue. In the above assays, we used PPTases in concentrations suitable for detection on SDS-PAGE gels. We also assayed PPTase bioactivity at a much lower concentration of *Mtb* PptT (0.1 μM) and 50 μM of *Mtb* apo-AcpM (500-fold excess over *Mtb* PptT) and at different time points. The enzymatic reactions were stopped by the addition of loading buffer and incubation at 90°C for 1 min. The conversion of *Mtb* apo-AcpM to *Mtb* holo-AcpM was analyzed by 15% SDS-PAGE.

Mass Spectrometry Analysis of *Mtb* apo-AcpM in the PPTase Enzymatic Assay. Samples from the PPTase bioassays above were electrosprayed in the positive mode using Q1 scan mode on a 4000 Q TRAPMass spectrometer (Applied Biosystems). The setting parameters were curtain gas

(CUR) 20; ionspray voltage (IS) 2800; declustering potential (DP) 120; entrance potential (EP) 10.

Blue Pigment Synthase Assay for PPTase Activity.^{34,35}

BpsA cloning and expression are described in the Supporting Information. A coupled assay of BpsA activation by PPTase followed by indigoidine production was performed in clear flat bottom 96-wells plates (Nunc, Denmark) at 25°C . The assay mixture included 5 mM MgCl₂, 5 mM ATP, 8 mM L-Gln, CoA (at a concentration range of 0.3–50 μM) and *Mtb* PptT (2 μM) or Sfp (0.2 μM) in a total volume of 100 μL of 100 mM Tris-HCl (pH 8.0). To initiate the reaction, 50 μL of BpsA (1 μM) was added, and the assay was monitored at 590 nm for 30 min at 20 s intervals. Five to six replicates were assayed. The change in absorbance at 590 nm was recorded using a Tecan Infinite 200 Pro reader. Raw data were analyzed with GraphPad Prism using Michaelis–Menten equation fit, and K_m and V_{max} were calculated.

ACP Competition Assay. Activation of BpsA from apo- to holo-BpsA by *Mtb* PptT was followed by a second stage of indigoidine synthesis. A 2-fold dilution series of each acyl carrier protein, *Mtb* AcpM or *C. striatum* AcpCS (16–0.125 μM) in 25 μL of a reaction buffer (400 nM CoA, 10 mM MgCl₂, 100 mM Tris-HCl, pH 8.0) was made in a 96-well microplate. A solution of apo-BpsA (5 μM in 25 μL reaction buffer) was then added to each well. Conversion into holo-BpsA was initiated by the addition of *Mtb* PptT (0.1–0.2 μM , in 50 μL reaction buffer). Plates were incubated for 30–60 min at room temperature. Indigoidine synthesis was initiated by the addition of a solution of L-Gln (10 mM) and ATP (5 mM) in 100 μL of the reaction buffer per well, and the absorption at 590 nm (A_{590}) was recorded every 20 s for 10 min using Tecan Infinite 200 PRO plate reader. Maximum velocity values for indigoidine synthesis were derived using the slope function of Microsoft Excel and converted into percentage maximum velocity values relative to the fastest reaction (without *Mtb* apo-AcpM) recorded for a duplicate experiment. In order to calculate IC₅₀ values, data for *Mtb* PptT/ACP combination were pooled, and four parameter dose–response curves were fitted using the nonlinear regression function of GraphPad Prism.

Binding Studies of *Mtb* PPTases to *Mtb* AcpM using Surface Plasmon Resonance (SPR).

Real-time interactions between *Mtb* apo-AcpM and *Mtb* PptT or *Mtb* AcpS were measured by SPR on a Biacore 3000 system at 25°C . The CMS (carboxymethylated dextran) chip was activated using an amine coupling reagent mixture of equal volumes of 50 mM N-hydroxysuccimide (NHS)/200 mM methyl-N-(3-diethylamino-propyl)-carboiimide (EDC) (Biacore, AB, Uppsala, Sweden) to form activated carboxyl groups. *Mtb* Apo-AcpM was diluted to a concentration of 50 $\mu\text{g}/\text{mL}$ in phosphate buffer saline pH 7.4 (137 mM NaCl, 2.7 mM KCl, 8 mM Na₂HPO₄, 2 mM KH₂PO₄) supplemented with 10 mM MgCl₂, 2% glycerol and immobilized on the chip, as recommended by the manufacturer. Ethanolamine-HCl (1.0M, pH 8.0) was used to neutralize unbound activated sites on the chip. Binding and kinetic assays were performed in the same phosphate buffer supplemented with 0.5 mM CoA or in the stabilizing buffer for *Mtb* PptT (50 mM MES pH 5.8, 500 mM NaCl, 10 mM MgCl₂, and 10% (v/v) glycerol buffer) reported by Vickery et al.²⁹ supplemented with 0.5 mM CoA. Kinetic analysis of the interaction between immobilized *Mtb* apo-AcpM and *Mtb* PptT was performed at concentrations ranging from 0–80 μM at a flow rate of 20 $\mu\text{L}/\text{min}$ for 4 min. Regeneration was performed with 8 mM NaOH

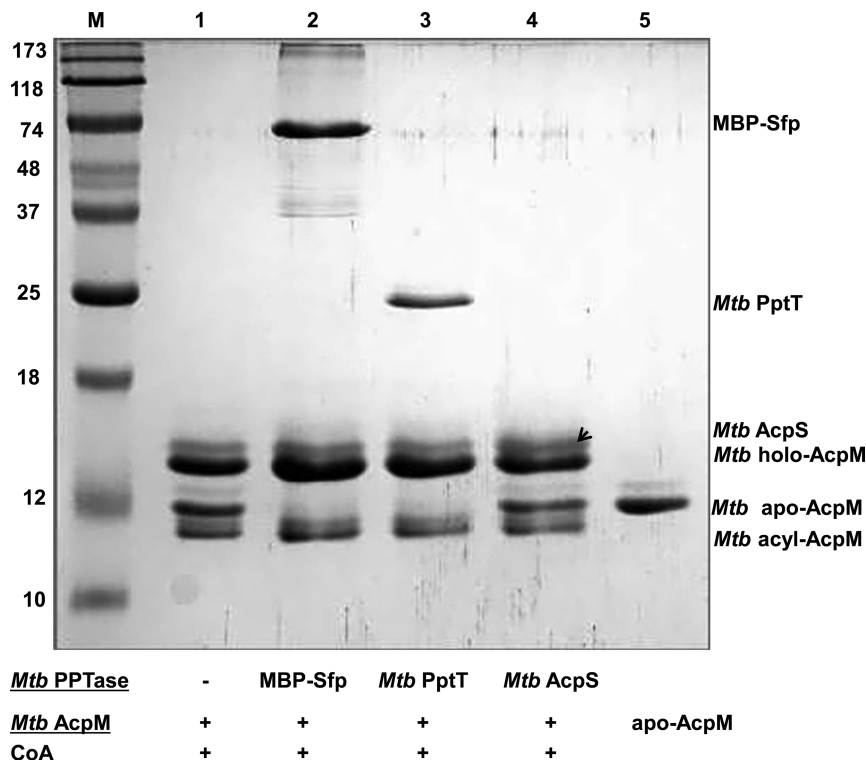


Figure 1. PPTase activity on purified *Mtb* AcpM mixture from *E. coli*. Each of the three PPTases, MBP-Sfp^{NEB}, *Mtb* PptT, and *Mtb* AcpS were mixed with *Mtb* AcpM at a molar ratio of 1:5. M indicates the molecular mass markers, lane 1: *Mtb* AcpM without PPTase, lane 2: *Mtb* AcpM with MBP-Sfp^{NEB}, lane 3: *Mtb* AcpM with *Mtb* PptT, lane 4: *Mtb* AcpM with *Mtb* AcpS (indicated by arrowhead), lane 5: purified *Mtb* apo-AcpM as a reference. The proteins were separated on 15%-SDS-Tris-PAGE and visualized with Coomassie Blue.

at a flow rate of 20 $\mu\text{L}/\text{min}$ for 1 min. The analysis was performed three times for each concentration. In order to exclude background, the results from the control surface were subtracted from that of *Mtb* apo-AcpM-immobilized surface. The response was monitored as a function of time (sensorgram). Sensograms were analyzed with BIA-evaluation software version 3.2 (Biacore). The dissociation constant (K_D) was derived from the kinetic analysis. Binding experiments of *Mtb* AcpM to *Mtb* AcpS or to BSA (as a control) were conducted in the same two buffer systems and by the same procedure described for *Mtb* PptT.

Structure-Based Sequence Alignment and Modeling of PptT–AcpM Complex. Multiple sequence alignment was carried out using the program ClustalW³⁶ and visualized by ESPript.³⁷ Structural models were prepared using PyMOL software (DeLano Scientific LLC).

RESULTS

Production of Native Full-Length *Mtb* PptT. The protein sequence of PptT from *M. bovis* BCG which was used in this study is identical to the sequences of tuberculosis bacilli *Mtb* CDC1551, *Mtb* SUMU002 and *M. africanum* GM041182. This *Mtb* PptT protein sequence differs from the sequence of *Mtb* strain H37Rv for which Met 87 is replaced by Val. Native *Mtb* PptT was reported to be poorly soluble in previous studies and was used as a soluble fusion protein with MBP.^{22,24} One study described the purification of native PptT in the presence of CoA and Mg²⁺, the substrate and cofactor for *Mtb* PptT activity.³⁸ A recent study of *Mtb* PptT structure reported that maximal thermal stability of *Mtb* PptT is obtained between pH 5.5–5.8 and at high salt concentration.²⁹ We empirically tested L-arginine for *Mtb* PptT purification

following reports of its ability to prevent aggregation.³³ L-Arginine was added to the purification protocol at a concentration of 0.25 M resulting in soluble native *Mtb* PptT suitable for bioactivity assays.

Phospho-pantetheinylation of *Mtb* AcpM by *Mtb* PptT. *Mtb* AcpM was expressed in either BL21 (DE3) strain or in BL21 (DE3) $\Delta entD$ strain lacking the native *E. coli* PPTase gene, *entD*, to exclude any effects of the *E. coli* host PPTase on *Mtb* AcpM during production.²¹ Purification of *Mtb* AcpM yielded three bands on SDS PAGE (Figure 1, lane 1), which were previously identified as *Mtb* apo-AcpM, *Mtb* holo-AcpM, and palmitoylated *Mtb* holo-AcpM.^{25,26} The faster electrophoretic mobility of an acylated compared to the nonacylated polypeptide was observed previously³⁹ and attributed to an increased binding of SDS, presumably due to a decrease in the net negative charge following acylation of the polypeptide.⁴⁰

The pattern of *Mtb* AcpM expression did not differ between the two *E. coli* strains, BL21 (DE3) and BL21 (DE3) $\Delta entD$ (data not shown), suggesting that the endogenous *E. coli* PPTase EntD unlike *E. coli* Acps^{25,26} does not affect *Mtb* AcpM. Therefore, the BL21 (DE3) strain was subsequently used for *Mtb* AcpM expression. To monitor PPTase activity, we initially used an *Mtb* AcpM mixture of the three forms, partially purified by Ni capture. We first followed the conversion of *Mtb* apo-AcpM to holo-AcpM by SDS PAGE in the presence and absence of purified *Mtb* AcpS, the PPTase that has been proposed for *Mtb* AcpM activation. Surprisingly, the addition of CoA with or without *Mtb* AcpS resulted in complete conversion of *Mtb* apo-AcpM to holo-AcpM (Supplementary Figure 1, lanes 3 and 4), whereas this reaction without CoA and in the presence of *Mtb* AcpS did not result in consumption of

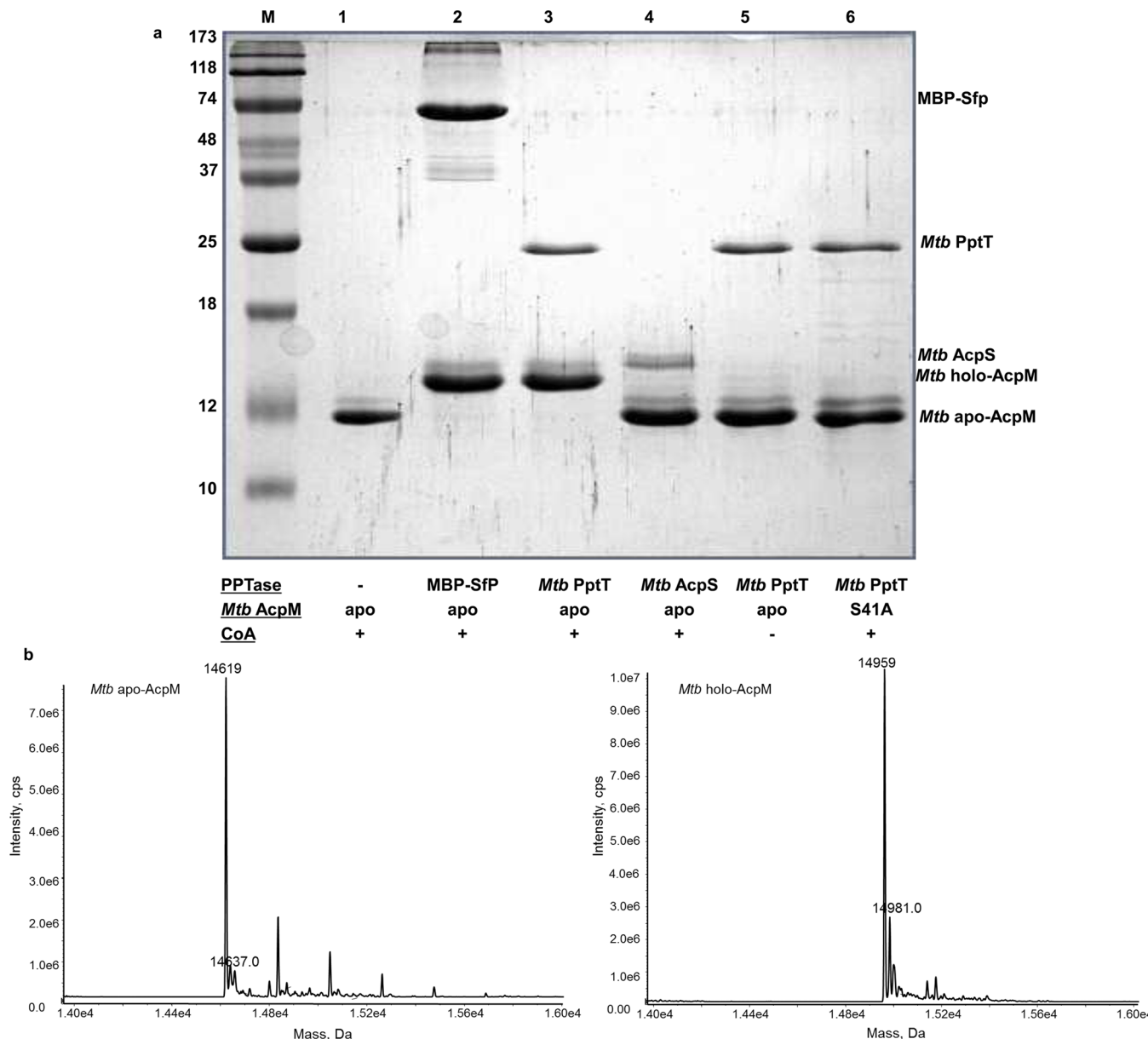


Figure 2. Analysis of *Mtb* apo-AcpM activation by PPTases. (a) MBP-Sfp^{NEB}, *Mtb* AcpS, and *Mtb* PptT were mixed each with *Mtb* apo-AcpM at a molar ratio of 1:5. M indicates the molecular mass markers, lane 1: *Mtb* apo-AcpM without PPTase, lane 2: *Mtb* apo-AcpM with MBP-Sfp^{NEB}, lane 3: *Mtb* apo-AcpM with *Mtb* PptT, lane 4: *Mtb* apo-AcpM with *Mtb* AcpS, lane 5: *Mtb* apo-AcpM with *Mtb* PptT and without CoA, lane 6: S41A *Mtb* AcpM mutant with *Mtb* PptT. The proteins were separated on 15% SDS-Tris PAGE and visualized with Coomassie Blue. (b) Electrospray mass spectrometry analysis of *Mtb* apo-AcpM (left panel), and *Mtb* holo-AcpM following activation by *Mtb* PptT (right panel). The expected mass of apo-*Mtb* AcpM is 14 620 Da for the *Mtb* AcpM fusion protein with the N-terminus from the vector following removal of methionine.²⁵ The calculated mass of *Mtb* holo-AcpM is 14 960 Da.

Mtb apo-AcpM (Supplementary Figure 1, lane 5). This finding suggested that partially purified *Mtb* AcpM might contain residual *E. coli* AcpS, which was below detection levels of the Coomassie Brilliant Blue staining, but was sufficient to complete the conversion of *Mtb* apo- to holo-AcpM in the presence of excess CoA. This finding prompted us to use a more stringent purification protocol for *Mtb* AcpM isolation, by adding a step of ion exchange followed by size exclusion chromatography to eliminate putative contamination of residual *E. coli* AcpS in the *Mtb* AcpM preparation. The purified *Mtb* AcpM mixture (containing the three forms *Mtb* apo, holo, and palmitoylated-holo AcpM) did not show a total conversion of *Mtb* apo- to *Mtb* holo-AcpM by merely adding CoA and Mg²⁺.

in the absence of an appropriate PPTase (Figure 1, lane 1). This observation supported the notion that residual *E. coli* AcpS from the *Mtb* AcpM preparation can exhibit background activity.

In order to identify the *Mtb* PPTase activator of *Mtb* AcpM, we tested the two *Mtb* PPTases, *Mtb* AcpS and *Mtb* PptT, and MBP-Sfp^{NEB} (a commercial MBP-Sfp synthase that activates ACP of *E. coli* as a positive control). We used the highly purified *Mtb* AcpM mixture as substrate and followed the conversion of *Mtb* apo-AcpM to *Mtb* holo-AcpM by the three enzymes using SDS PAGE (Figure 1). Both *Mtb* PptT and Sfp^{NEB} resulted in complete consumption of the *Mtb* apo-AcpM band and in the enhancement of the protein band

corresponding to *Mtb* holo-AcpM (Figure 1, lanes 2 and 3), whereas purified *Mtb* AcpS did not appear to affect the level of the *Mtb* apo-AcpM (Figure 1, lane 4). These results suggested that *Mtb* PptT is the *Mtb* PPTase activator of *Mtb* AcpM. It should be noted that the *Mtb* AcpS used in all our experiments is the same preparation used to analyze its crystal structure (PDB code 3HQJ),²⁷ leading to unambiguous identification of the 3',5'-ADP moiety, the product of CoA cleavage by the active *Mtb* AcpS. The activity of *Mtb* AcpS was also demonstrated by mass spectrometry analysis of peptides following trypsin and chymotrypsin digestion of FAS I activated by AcpS supporting the covalent binding of 4'-PP to Serine residue in position 1833 (data not shown).

Following the activation results obtained for the *Mtb* AcpM mixture described above, we then subjected the pure apo-AcpM fraction to the three enzymes: *Mtb* AcpS, *Mtb* PptT, and MBP-Sfp^{NEB}. A possible effect of residual *E. coli* AcpS activity was ruled out again by the addition of CoA to *Mtb* apo-AcpM in the absence of any PPTase (Figure 2a, lane 1). Complete conversion of *Mtb* apo-AcpM into holo-AcpM was observed only upon addition of Sfp^{NEB} or *Mtb* PptT (Figure 2a, lanes 2, 3), whereas *Mtb* AcpS did not affect *Mtb* apo-AcpM (Figure 2a, lane 4). The conversion of *Mtb* apo-AcpM to *Mtb* holo-AcpM in the presence of *Mtb* PptT was abolished in the absence of CoA (Figure 2a, lane 5), confirming that *Mtb* apo-AcpM conversion to *Mtb* holo-AcpM was a result of the *in vitro* PPTase activity and not due to residual contamination of CoA from the protein purification process.

An analysis of *Mtb* AcpM prior to and following its activation by *Mtb* PptT was performed by ES-MS, showing a mass shift of 340 Da (the expected mass of 4'-PP) in *Mtb* apo-AcpM upon activation by *Mtb* PptT. The expected mass of *Mtb* apo-AcpM fusion protein with the N-terminus from the vector following removal of methionine²⁵ is 14 620 Da, and the calculated mass of *Mtb* holo-AcpM is 14 960 Da. The expected mass of 4'-PP is 340 Da thereby confirming the transition from *Mtb* apo-AcpM (Figure 2b, left panel) to *Mtb* holo-AcpM (Figure 2b, right panel). The PPTase assays displayed in Figures 1 and 2 were done at a 1–5 molar ratio of PPTase to *Mtb* AcpM to enable the detection of both *Mtb* AcpM and the specific PPTase by SDS-PAGE. However, PPTases have been reported to activate their ACP substrates at a much higher molar ratio of ACP to PPTase with increased accumulation of holo-ACP following longer incubation.²⁶ Indeed, *Mtb* PptT activated *Mtb* apo-AcpM at a molar ratio of 1–500 showing increased accumulation of *Mtb* holo-AcpM over time as expected (Supplementary Figure 2) in agreement with previous studies of PPTase activation *in vitro*.

Ser41 of *Mtb* AcpM Is the Active Residue That Undergoes 4' Phospho-pantetheinylation by PPTases. It was suggested that Ser41 within the conserved DSL motif (D40-S41-L42) is the activated serine based on the solution structure of *Mtb* AcpM by NMR spectroscopy.¹¹ Most ACPs have an Asp43 residue following Leu42 in the DSL motif. However, in mycobacteria and corynebacteria the corresponding residue following DSL is Ser43.²⁷ To test whether Ser41 of *Mtb* AcpM is indeed the conserved serine residue critical for 4'-PP transfer by either *E. coli* AcpS or *Mtb* PptT, we expressed and purified the corresponding S41A mutant of *Mtb* AcpM. Expression of this mutant in *E. coli* yielded a single protein of the correct size that was not affected by excess CoA (as identified by SDS PAGE shown in Supplementary Figure 3, lanes 3 and 4 and by mass spectrometry analysis, data not

shown). The expression of S41A mutant of *Mtb* AcpM as a single protein is in contrast to the identification of a mixture of apo-, holo-, and acylated holo-AcpM, following expression of wild type *Mtb* AcpM resulting from the host *E. coli* AcpS activity.²⁵ The S41A mutation abolished activation of *Mtb* AcpM by *Mtb* PptT (Figure 2a, lane 6), confirming the critical role of Ser41 in 4'-PP transfer by the corresponding PPTases.

C. striatum PptCS Activates *Mtb* AcpM. Previous studies showed that disruption of *pptT* in mycobacteria is lethal and that *pptCG* of *C. glutamicum* could complement a strain of *M. smegmatis* following *pptT* disruption.²¹ On the basis of the observed successful complementation by *pptCG*, it can be expected that a PptT from a corynebacteria species could activate *Mtb* AcpM. We expressed the PptT ortholog from *C. striatum* (PptCS) and tested its activity on *Mtb* AcpM. PptCS is a 222 amino-acid long protein that has an amino acid sequence identity of 42% with *Mtb* PptT and 65% with PptGC of *C. glutamicum* ATCC 13032. As expected, PptCS completed conversion of *Mtb* apo-AcpM to *Mtb* holo-AcpM in a typical PPTase assay as described above (Figure 3). This finding supports the concept of common catalytic functions for the broad spectrum PPTases of mycobacteria and corynebacteria.

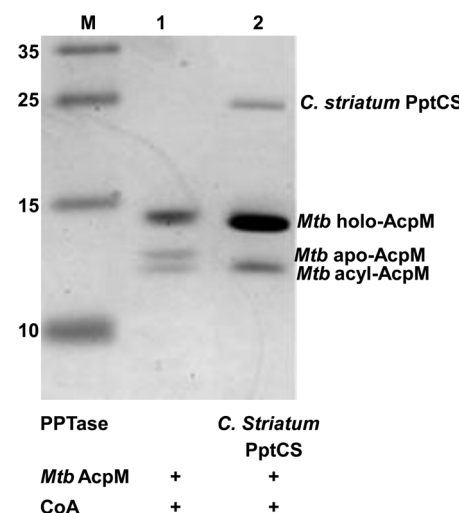


Figure 3. *C. striatum* Ppt (PptCS) activity on *Mtb* AcpM. M indicates the molecular mass marker lane 1: *Mtb* AcpM, lane 2: *C. striatum* PptCS with *Mtb* AcpM at a ratio of 1:5. The proteins were separated on 15% -SDS- Tris PAGE and visualized with Coomassie Blue.

Kinetic Parameters of *Mtb* PptT Using BpsA as a Reporter. We adopted the previously published BpsA assay to monitor PPTase activity.³⁴ BpsA is a pigment producing NRPS (from *Streptomyces lavendulae*) that requires activation from an apo to a holo form by a broad spectrum PPTase. The holo-BpsA catalyzes the conversion of two molecules of L-glutamine into indigoidine, a blue pigment that can be detected at 590 nm.³⁵ The rate of indigoidine synthesis is directly proportional to the concentration of holo-BpsA, thereby enabling the derivation of kinetic parameters for PPTase with respect to CoA or BpsA itself as a variable substrate. We used this assay for determining *Mtb* PptT activity in comparison to that of MBP-Sfp^{NEB}, using CoA as the variable substrate.

K_m and k_{cat} values for the two enzymes as derived from a Michaelis–Menten fit (Figure 4a) were $3.9 \pm 0.8 \mu\text{M}$ and $0.83/\text{min}$ for *Mtb* PptT; $3.4 \pm 0.6 \mu\text{M}$ and $3.8/\text{min}$ for MBP-Sfp. The relatively slow catalytic activity of *Mtb* PptT, also shown by

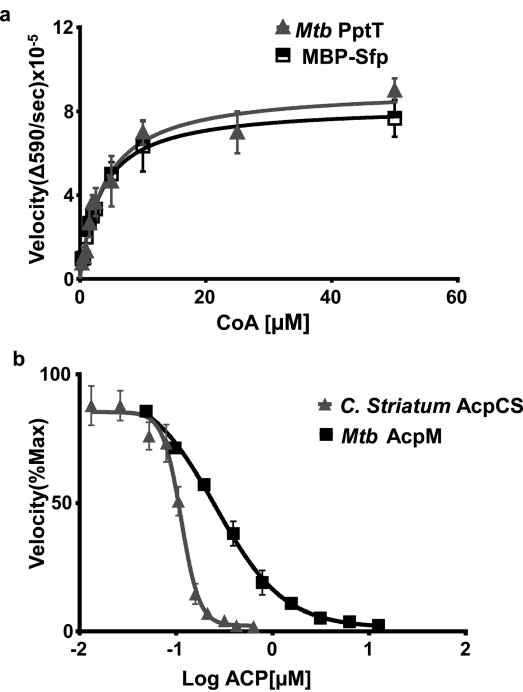


Figure 4. (a) Kinetic analyses of *Mtb* PptT and MBP-Sfp^{NEB}. Michaelis–Menten fit of *Mtb* PptT (triangles) and MBP-Sfp^{NEB} (squares) with CoA as the variable substrate in a BpsA activity assay. Error bars are presented as \pm SEM. (b) ACP competition assay. IC₅₀ curve for *Mtb* PptT competition assay. Pooled data for three replicates at each *Mtb* AcpM and *C. striatum* AcpcS concentration are shown, and error bars are presented as \pm SEM. Four-parameter dose–response curves were obtained using GraphPad Prism software.

other studies,^{24,29} is likely related to its particularly broad range of carrier protein substrates: acyl carrier protein domains of polyketide synthases, peptidyl and aryl carrier domains (PCP and ArCP) of nonribosomal peptide synthases and AcpM protein. This broad range may reduce specialization and efficiency of its catalytic activity toward individual substrates.

Competition Assay of ACP with BpsA for Limited CoA.

A competition assay in which BpsA and purified *Mtb* apo-ACP are converted to their holo forms using a limited pool of CoA can be used to assess the relative efficiency of apo-ACP conversion by its PPTase. In the first stage, holo-ACP formation results in less holo-BpsA that will be detected as diminished indigoindine synthesis when ATP and L-glutamine are added in the second stage. We measured the IC₅₀ for *Mtb* AcpM and a modified related *C. striatum* ACP, AcpcS (described in Supplementary Figure 4). The corresponding values are $0.26 \pm 0.06 \mu\text{M}$ and $0.11 \pm 0.01 \mu\text{M}$, respectively (Figure 4b). We propose that the lower IC₅₀ for *C. striatum* ACP compared to *Mtb* AcpM results from a higher rate of ACP activation required for a fast growing corynebacteria species compared to the slow growing tuberculous bacilli.

***Mtb* PptT Interaction with *Mtb* AcpM Demonstrated by Surface Plasmon Resonance (SPR).** To study the binding interaction of each of the two *Mtb* PPTases, PptT and AcpS, with *Mtb* AcpM which likely underlies their different activity toward *Mtb* AcpM described above, we used the SPR method. The data collected from SPR experiments show specific binding between the immobilized *Mtb* apo-AcpM and the injected *Mtb* PptT (Figure 5a). By contrast, when *Mtb* AcpS or bovine serum albumin (BSA) were injected under the

same conditions, no binding was detected (Figure 5b). The binding constant K_D derived from the kinetic data of *Mtb* PptT is close to $40 \mu\text{M}$, indicating an attractive interaction between *Mtb* apo-AcpM and *Mtb* PptT. No comparable binding studies between ACPs and PPTases were reported. Although no binding between *Mtb* AcpS and *Mtb* AcpM was detected by SPR, weak binding below the detection limit of this method cannot be excluded.

Sequence-Structure Alignment of *Mtb* PptT with Other Sfp-type PPTases and Modeling of *Mtb* PptT Interaction with *Mtb* AcpM.

Mtb PptT belongs to the class of Sfp-type PPTases which are monomers of 240 amino acids. The crystal structures of Sfp from *B. subtilis* (Sfp) and human PPTase PPT Hs (PDB codes 1QR0 and 2BYD, respectively) have been previously determined.^{15,24,41} Despite the low sequence identity (22%) between *B. subtilis* Sfp and PPT Hs their monomers display a similar fold composed of two domains, each with approximately 120 residues, showing a pseudo 2-fold symmetry. Each of the domains of Sfp and PPT Hs is characterized by an α/β fold similar to the architecture observed for each of the *Mtb* AcpS monomers (120 amino acid long) and other AcpS-type PPTases.^{14,42} While Sfp-type PPTases are functional as monomers, the AcpS-type PPTases are functional as homotrimers.^{14,27} The homology of these broad spectrum PPTases to *Mtb* PptT is low with sequence identity of 13.2% to Sfp and 13.9% with many gaps to PPT Hs as shown by the aligned members of the Sfp-type PPTases displaying only six strictly conserved residues (red boxes in Figure 6a). Despite the low sequence identity between *Mtb* PptT and either PPT Hs or Sfp, *Mtb* PptT adopts a similar α/β fold with a pseudo 2-fold symmetry between the two domains as observed in the recent crystal structure of *Mtb* PptT.²⁹ Most of the strictly conserved residues: Pro72, Ser90, Glu134, Lys156, Glu157, and Lys161 (*Mtb* PptT numbering in Figure 6a) have defined structural roles. Two of the invariant residues Glu134 and Lys156 participate in a conserved intramolecular salt bridge present in all known Sfp-type and AcpS-type PPTase structures. Two other strictly conserved residues, Lys161 and Glu157, have a primary role in CoA binding and ACP activation in the two PPTase classes.^{14,27} On the basis of the *Mtb* PptT structure²⁹ and on the sequence alignment (Figure 6a), it appears that these conserved residues have the same role in *Mtb* PptT as in other Sfp-type PPTases.

To generate a structural model of the complex of *Mtb* PptT with *Mtb* AcpM, the X-ray structure of *Mtb* PptT (PDB code 4QJK) and the NMR structure of *Mtb* AcpM (PDB code 1KLP)¹¹ were each superposed onto the crystal structure of the PPT Hs in complex with the ACP domain of the human FAS and CoA (PDB code 2CG5)⁴¹ shown in Figure 6b. The model of the *Mtb* complex also shown in Figure 6c demonstrates that *Mtb* AcpM (in magenta) binds at the cleft formed by the two domains of *Mtb* PptT (in orange and green), in a manner that most of the short intermolecular contacts involve residues from the N-terminal domains of both *Mtb* PptT and *Mtb* AcpM, supporting several stabilizing interactions. These include hydrophobic interactions between Val45 from *Mtb* PptT and Val34 from *Mtb* AcpM as well as electrostatic interactions involving basic residues of *Mtb* PptT (Arg43, Lys47, and Arg48) and acidic residues of *Mtb* AcpM (Asp35, Asp36, and Asp38) shown in Figure 6c. The positively charged patch of *Mtb* PptT can interact with the negatively charged region of *Mtb* AcpM as demonstrated by the electrostatic representation of the *Mtb* complex shown in Figure 6d. These findings suggest

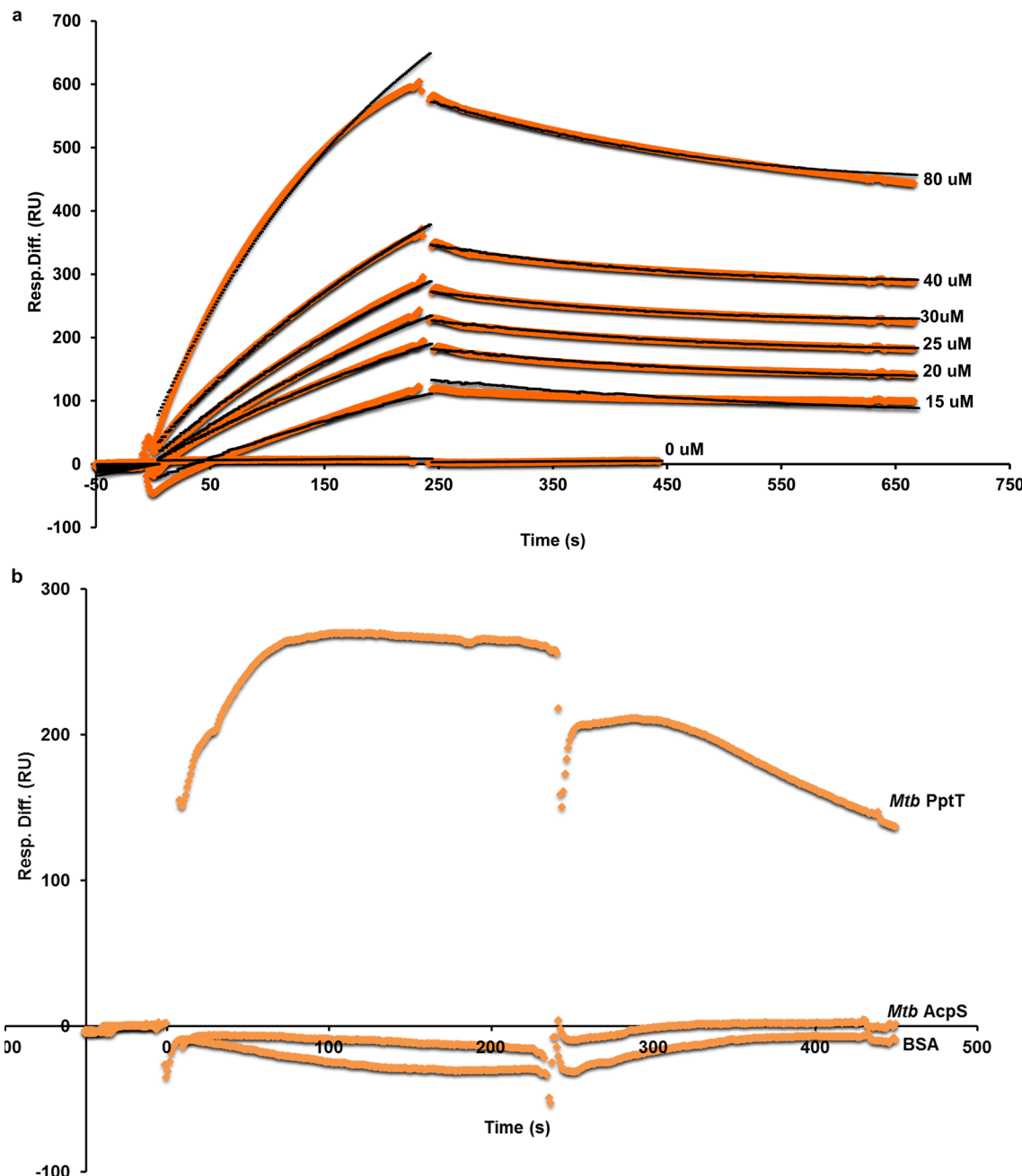


Figure 5. Measurements of binding interactions by SPR. (a) SPR sensograms of *Mtb* PptT, injected at six different concentrations at a flow rate of 20 μ L/min over immobilized apo-AcpM. Injection of the *Mtb* PptT concentration series was repeated three times. A 1:1 binding model (black lines) was fitted and displayed on the raw data (orange). (b) SPR sensograms comparing the binding of immobilized *Mtb* AcpM to *Mtb* PptT, *Mtb* AcpS, and BSA. All three proteins were injected at a concentration of 20 μ M at a flow rate of 20 μ L/min for 4 min.

that both hydrophobic and electrostatic interactions could stabilize the interaction between enzyme and substrate, thereby facilitating activation of *Mtb* AcpM by *Mtb* PptT.

■ DISCUSSION

This study shows that *Mtb* PptT a broad spectrum Sfp-like PPTase is the mycobacterial PPTase that activates *Mtb* AcpM, the ACP for meromycolate extension, a fundamental activity for mycobacterial cell wall biosynthesis and a proven drug target.^{6,43} To date, activation of a highly purified *Mtb* AcpM has not been assessed directly using isolated *Mtb* AcpS or *Mtb* PptT. We show that by subjecting *Mtb* AcpM to the activity of the two *Mtb* PPTases, AcpS and PptT, only *Mtb* PptT converts

Mtb apo-AcpM to *Mtb* holo-AcpM. The conversion of *Mtb* apo-AcpM to *Mtb* holo-AcpM is through a conserved Ser41 residue of the DSL motif and can be conducted at a high molar ratio of *Mtb* AcpM to *Mtb* PptT, as is expected for PPTases. The finding that *Mtb* AcpS does not activate *Mtb* AcpM, whereas *E. coli* AcpS does, may appear counterintuitive, but it is in agreement with our previous analysis of the crystal structure of *Mtb* AcpS which exhibited unique properties in comparison to AcpSes from other species. We showed that *Mtb* AcpS, unlike other bacterial species, does not possess the conserved basic residues necessary for interaction with ACPs.²⁷ The *B. subtilis* complex structure of AcpS with its ACP is stabilized by electrostatic interactions contributed by three key residues from

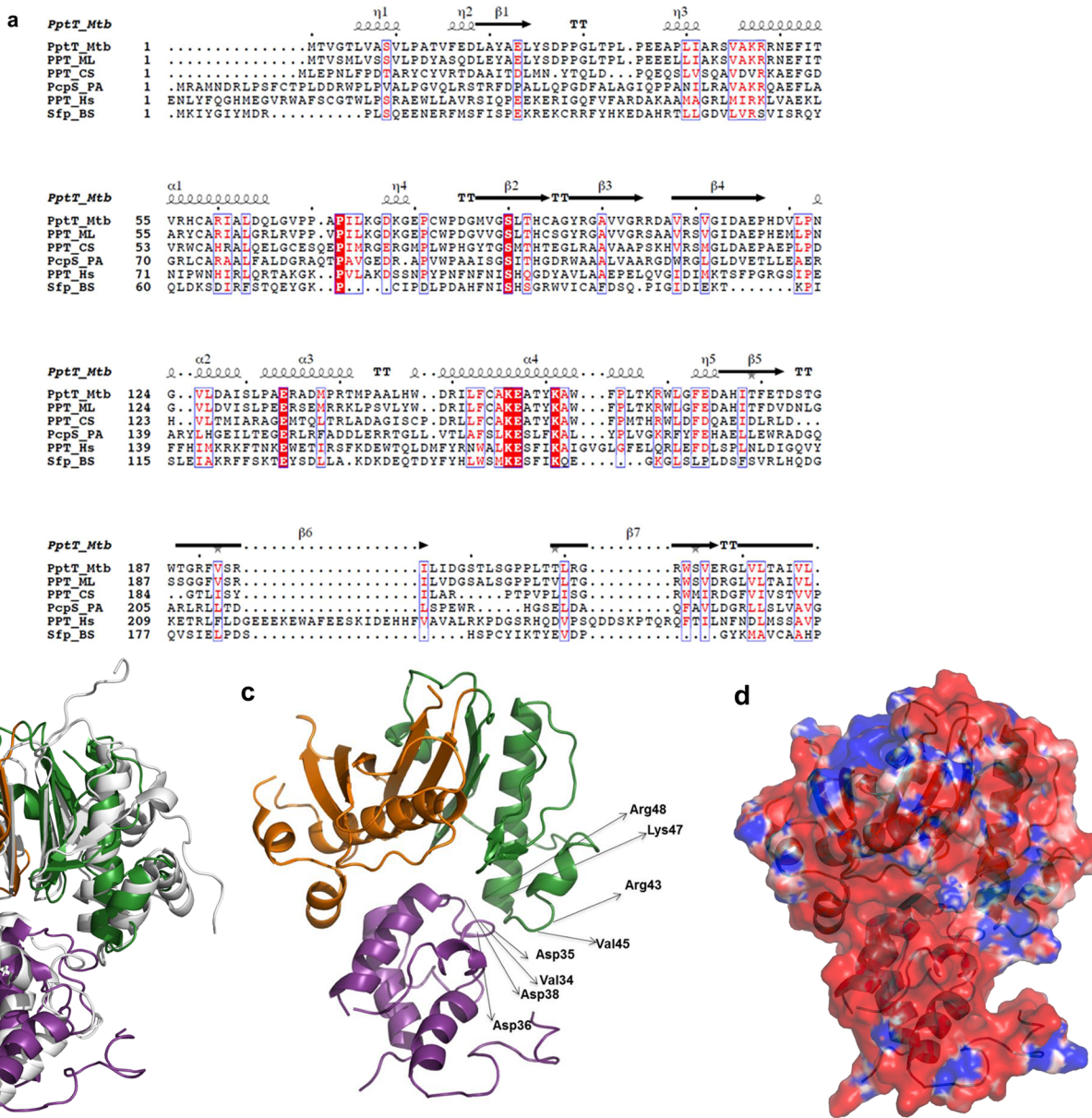


Figure 6. Sequence-structure analysis of *Mtb* PptT and its complex with *Mtb* AcpM. (a) Structure-based sequence alignment of *Mtb* PptT with other Sfp like PPTases. This includes the PptTs from the corynebacterineae family: *M. tuberculosis* (PptT_Mtb), *M. leprae* (PPT_ML), *C. striatum* (PPT_CS), and the PcpS of *P. aeruginosa* (PcpS_PA), *B. subtilis* (Sfp_BS, PDB code: 1QR0) and *Homo sapiens* (PPT_Hs, PDB code: 2BYD). Secondary structures are labeled above the corresponding sequence; α -helices are depicted by spirals and β -strands by arrows. The strictly conserved residues in all proteins are highlighted in red, and similar residues appear in blue boxes. (b) Structural model of *Mtb* PptT bound to *Mtb* AcpM superposed on the crystal structure of the complex between PPT Hs and ACP. Structure of the *Mtb* complex was obtained by the superposition of the *Mtb* PptT crystal structure (PDB code 4QJK) and the NMR structure of *Mtb* AcpM (PDB code 1KLP), onto the known complex structure of PPT Hs with ACP domain (PDB code 2CG5). The two domains of the PptT structure (PDB code 4QJK) are shown in orange and green, the *Mtb* AcpM is shown in magenta, and the reference structure is in gray. (c) The structural model of *Mtb* PptT bound to *Mtb* AcpM showing the structural complementarity between the two proteins. The color code is as in b. The hydrophobic and charged residues at the molecular surfaces that are predicted to stabilize the complex are indicated. (d) Electrostatic representation of *Mtb* PptT bound to *Mtb* AcpM. The electrostatic potential is mapped on the molecular surface of *Mtb* complex (negative potential in red and positive potential in blue). The orientation of the complex is the same as in panel c. The N-terminal domain of *Mtb* PptT structure displays an electropositive patch at the cleft formed by the two domains. This patch formed by positively charged Arg and Lys residues (shown at the right-handed side of the image) is predicted to interact with the electronegative regions of *Mtb* AcpM formed by Asp residues (indicated in panel c).

AcpS Arg15, Arg22, and Arg29 that are involved in salt bridge contacts with acidic residues from ACP. The same basic residues are conserved in *E. coli* AcpS and in other species as well.^{14,27} Therefore, it is likely that similar stabilizing interactions will take place between the electropositive surface of *E. coli* AcpS and the electronegative surface of *Mtb* AcpM.

accounting for the activation of partially purified *Mtb* AcpM from *E. coli*. By contrast, *Mtb* AcpS does not have the conserved three basic residues for supporting the described interaction with ACPs.²⁷ Moreover, these basic residues are substituted by acidic residues in *Mtb* AcpS: Asp15, Gln22, and Glu29. Notably, the same acidic residues are conserved among other

corynebacterine family members. The electronegative surface formed by such residues in *Mtb* AcpS is expected to promote repulsion with the electronegative surface of *Mtb* AcpM and thereby destabilize their complex.²⁷ Unlike *Mtb* AcpS, our structural model of *Mtb* PptT bound to *Mtb* AcpM shows structural complementarity between the two proteins favoring both hydrophobic and electrostatic interactions between them.

The finding that *Mtb* PptT activates *Mtb* AcpM agrees with the current canonical classification of PPTase function, in which AcpSes activates either FAS I or FAS II systems.¹⁷ The *Mtb* *acpS* gene (*Rv2524*) is located downstream of *Mtb* *fas* (*Rv2523*). An *in vitro* study of transcription regulation of fatty acid biosynthesis in mycobacteria have shown that *Mtb* *fas* and *acpS* genes are part of the same transcription unit forming a *fas1-acpS* operon under the control of FasR, an essential transcription regulator.⁴⁴ The functional association of *Mtb* AcpS with *Mtb* FAS I is further supported by the structure-function organization of the analogous yeast FAS I which possesses an AcpS domain as part of the unit of the α/β dodecamer complex.^{18,20} Unlike AcpSes, Sfp-type PPTases usually function in secondary metabolism such as meromycolate extension for mycobacteria.¹⁷ However, some broad spectrum Sfp-like PPTases also activate ACP of the FAS II system. Most notably, *Pseudomonas* species have only one broad spectrum Sfp-like PPTase and lack AcpS. This PPTase affects both fatty acid and siderophore synthesis.⁴⁵ Thus, *Mtb* AcpM activation by *Mtb* PptT, which is a broad spectrum Sfp-like PPTase, is not exclusive to mycobacteria and agrees with its established role for secondary metabolism. Therefore, our results support the concept that AcpSes are linked to fatty acid synthesis as activators of either FAS I or FAS II, but not of both. By contrast, the activity spectrum of broad spectrum Sfp synthase like PPTase for enzymes in secondary metabolism such as meromycolate synthesis and modification in mycobacteria may be extended in certain species (such as *Pseudomonas*) to primary metabolism of fatty acid synthesis through the ACP protein of the FAS II system.^{17,45} Dual activity of *Mtb* AcpS toward both *Mtb* FAS I and *Mtb* AcpM with redundant activation of *Mtb* AcpM by both *Mtb* AcpS and *Mtb* PptT appears unlikely in view of the results of the aforementioned structure-function study²⁷ and the data presented here.

The finding that *Mtb* PptT activates *Mtb* AcpM may also explain the results of the phenotype obtained following *pptT* gene disruption and complementation in mycobacteria and corynebacteria. The rescue of *M. smegmatis* Δ *pptT* strain by *pptCG* suggests that a PptT analogue from the corynebacteria species would activate *Mtb* AcpM as well. Indeed, the *Mtb* PptT ortholog PptTCS from *C. striatum* converted *Mtb* apo-AcpM to *Mtb* holo-AcpM in agreement with this concept of common catalytic functions for PPTases from mycobacteria and corynebacteria.²² In addition, our biochemical data suggest that *pptT* gene disruption will result in a nonfunctional *Mtb* AcpM protein in addition to PKS13 and thus provides a more comprehensive explanation to the lethality conferred by *pptT* gene deletion. Moreover, activation of *Mtb* AcpM may also explain the recent observation that *Mtb* PptT is required for replication and survival of tuberculous bacilli during the acute and chronic phases of infection in mice.²² Inactivation of *pptT* gene resulting in inactive *Mtb* AcpM is expected to completely impede meromycolate production and modification leading to arrest of *Mtb* multiplication.²²

The catalytic activity of PPTase was usually measured by quantitative analysis of substrate consumption or products

formation by HPLC or by radiolabeling.^{17,26,45} Spectrophotometric assays for high throughput screening of PPTase inhibitors^{46,47} based on binding of CoA-fluorophore labeled conjugates and scintillation proximity assay (SPA) for *Mtb* PptT activity were demonstrated.²² Fluorophore-CoA conjugates are not the natural substrate for PPTases and SPA requires radiolabeling. We used a simple colorimetric assay based on the production of a blue pigment indigoidine by a PPTase-activated BpsA (a nonribosomal peptide synthase, NRPS).³⁵ Using the BpsA assay we demonstrated that activation of ACPs, *Mtb* apo-AcpM, and a related *C. striatum* apo-ACP competes with BpsA on limited CoA, providing a quantitative measure of *Mtb* PptT activity toward ACP substrates.

The functional role of *Mtb* PptT as the PPTase that activates *Mtb* AcpM was further investigated by binding studies between *Mtb* AcpM and either *Mtb* PptT or *Mtb* AcpS, using SPR. Significant interaction with *Mtb* AcpM was observed only for *Mtb* PptT, in support of the activity studies and the predicted intermolecular interactions based on our sequence-structure analysis.

To gain insight into the molecular and structural basis of the interaction between *Mtb* PptT and *Mtb* AcpM, we presented a structural model of *Mtb* PptT bound to *Mtb* AcpM showing the structural complementarity between the two molecules and that both hydrophobic and electrostatic interactions at the cleft formed by the two domains of *Mtb* PptT appear to contribute to the integrity of the complex.

Mycolic acid biosynthesis is an established target for antituberculous first and second line agents, isoniazid and ethionamide that inhibit InhA, the enoyl reductase of the FAS II system.^{48,49} Recently, the therapeutic potential of simultaneous inhibition of multiple protein targets in the mycolate biosynthesis pathway was documented using a combination of thiophene, a new inhibitor of PKS13 and isoniazid resulting in enhanced sterilizing activity.⁵⁰ This finding demonstrated the effect that is expected from *Mtb* PptT inhibition.

To conclude, our finding that *Mtb* PptT is the sole activator of *Mtb* AcpM redefines its role as the PPTase for mycolic acid biosynthesis and thus expands its potential as a drug target affecting a multistep pathway.

ASSOCIATED CONTENT

S Supporting Information

Supplementary methods; Supplementary Table 1: application primers using for cloning; Supplementary Figure 1: partially purified (Ni beads) *Mtb* AcpM from *E. coli* in PPTase assay with *Mtb* AcpS. Supplementary Figure 2: *Mtb* PptT activity at high ratio of *Mtb* AcpM to *Mtb* PptT as a function of time. Supplementary Figure 3: activation assay of the S41A *Mtb* AcpM mutant compared to *Mtb* apo AcpM. Supplementary Figure 4: activation of *C. striatum* ACP (AcpCS). Supplementary Figure 5: a typical raw data of *Mtb* apo-AcpM competition in BpsA assay. This material is available free of charge via the Internet at <http://pubs.acs.org>.

AUTHOR INFORMATION

Corresponding Author

*E-mail: oren_z@clalit.org.il; Oren.Zimhony@weizmann.ac.il. Tel: 9729441993. Fax: 97289440081.

Author Contributions

[†]These authors (O.Z. and A.S.) made an equal contribution.

Funding

This work was supported by the Legacy Heritage Clinical Research Initiative of the Israel Science Foundation Grant No. 1629/10 to O.Z. and by the Israeli Ministry of Health Chief Scientist Award No. 6223 to O.Z. and Y.B.

Notes

The authors declare no competing financial interest.

#Deceased, April 2012.

ACKNOWLEDGMENTS

This project was supported by the Kimmelman Center for Macromolecular Structure and Assembly. Z.S. holds the Helena Rubinstein Professorial Chair in Structural Biology. The ISPC is supported by the Dana and Yossie Hollander Center for Structural Biology. We thank Ron Diskin for helpful discussions.

ABBREVIATIONS

Mtb, *Mycobacterium tuberculosis*; FA, fatty acid; 4'-PP, 4'-phosphopantetheinyl; ACP, acyl carrier protein; PPTase, 4'-PP transferase; FAS, fatty acid synthase; PKS, polyketide synthase; AcpS, acyl carrier protein synthase; NRPS, nonribosomal peptide synthase; BS, *Bacillus subtilis*; BpsA, blue pigment synthase A; BSA, bovine serum albumin

REFERENCES

- (1) World Health Organization. (2014) Tuberculosis Fact Sheet 104; <http://www.who.int/mediacentre/factsheets/fs104/en/index.html>.
- (2) Dao, D. N., Sweeney, K., Hsu, T., Gurcha, S. S., Nascimento, I. P., Roshevsky, D., Besra, G. S., Chan, J., Porcelli, S. A., and Jacobs, W. R. (2008) Mycolic acid modification by the mmaA4 gene of *M. tuberculosis* modulates IL-12 production. *PLoS Pathog.* 4, e1000081.
- (3) Glickman, M. S., Cox, J. S., and Jacobs, W. R., Jr. (2000) A novel mycolic acid cyclopropane synthetase is required for cording, persistence, and virulence of *Mycobacterium tuberculosis*. *Mol. Cell* 5, 717–727.
- (4) Takayama, K., Wang, C., and Besra, G. S. (2005) Pathway to synthesis and processing of mycolic acids in *Mycobacterium tuberculosis*. *Clin. Microbiol. Rev.* 18, 81–101.
- (5) Cole, S. T., Brosch, R., Parkhill, J., Garnier, T., Churcher, C., Harris, D., Gordon, S. V., Eiglmeier, K., Gas, S., Barry, C. E., 3rd, Tekaia, F., Badcock, K., Basham, D., Brown, D., Chillingworth, T., Connor, R., Davies, R., Devlin, K., Feltwell, T., Gentles, S., Hamlin, N., Holroyd, S., Hornsby, T., Jagels, K., Krogh, A., McLean, J., Moule, S., Murphy, L., Oliver, K., Osborne, J., Quail, M. A., Rajandream, M. A., Rogers, J., Rutter, S., Seeger, K., Skelton, J., Squares, R., Squares, S., Sulston, J. E., Taylor, K., Whitehead, S., and Barrell, B. G. (1998) Deciphering the biology of *Mycobacterium tuberculosis* from the complete genome sequence. *Nature* 393, 537–544.
- (6) Bhatt, A., Molle, V., Besra, G. S., Jacobs, W. R., Jr., and Kremer, L. (2007) The *Mycobacterium tuberculosis* FAS-II condensing enzymes: their role in mycolic acid biosynthesis, acid-fastness, pathogenesis and in future drug development. *Mol. Microbiol.* 64, 1442–1454.
- (7) Schweizer, E., and Hofmann, J. (2004) Microbial type I fatty acid synthases (FAS): major players in a network of cellular FAS systems. *Microbiol. Mol. Biol. Rev.* 68, 501–517.
- (8) Boehringer, D., Ban, N., and Leibundgut, M. (2013) 7.5-Å cryo-EM structure of the mycobacterial fatty acid synthase. *J. Mol. Biol.* 425, 841–849.
- (9) Kolattukudy, P. E., Fernandes, N. D., Azad, A. K., Fitzmaurice, A. M., and Sirakova, T. D. (1997) Biochemistry and molecular genetics of cell-wall lipid biosynthesis in mycobacteria. *Mol. Microbiol.* 24, 263–270.
- (10) White, S. W., Zheng, J., Zhang, Y. M., and Rock (2005) The structural biology of type II fatty acid biosynthesis. *Annu. Rev. Biochem.* 74, 791–831.
- (11) Wong, H. C., Liu, G., Zhang, Y. M., Rock, C. O., and Zheng, J. (2002) The solution structure of acyl carrier protein from *Mycobacterium tuberculosis*. *J. Biol. Chem.* 277, 15874–15880.
- (12) Quadri, L. E., Weinreb, P. H., Lei, M., Nakano, M. M., Zuber, P., and Walsh, C. T. (1998) Characterization of Sfp, a *Bacillus subtilis* phosphopantetheinyl transferase for peptidyl carrier protein domains in peptide synthetas. *Biochemistry* 37, 1585–1595.
- (13) Mootz, H. D., Finking, R., and Marahiel, M. A. (2001) 4'-Phosphopantetheine transfer in primary and secondary metabolism of *Bacillus subtilis*. *J. Biol. Chem.* 276, 37289–37298.
- (14) Parris, K. D., Lin, L., Tam, A., Mathew, R., Hixon, J., Stahl, M., Fritz, C. C., Sehra, J., and Somers, W. S. (2000) Crystal structures of substrate binding to *Bacillus subtilis* holo-(acyl carrier protein) synthase reveal a novel trimeric arrangement of molecules resulting in three active sites. *Structure* 8, 883–895.
- (15) Reuter, K., Mofid, M. R., Marahiel, M. A., and Ficner, R. (1999) Crystal structure of the surfactin synthetase-activating enzyme sfp: a prototype of the 4'-phosphopantetheinyl transferase superfamily. *EMBO J.* 18, 6823–6831.
- (16) Mofid, M. R., Finking, R., Essen, L. O., and Marahiel, M. A. (2004) Structure-based mutational analysis of the 4'-phosphopantetheinyl transferases Sfp from *Bacillus subtilis*: carrier protein recognition and reaction mechanism. *Biochemistry* 43, 4128–4136.
- (17) Lambalot, R. H., Gehring, A. M., Flugel, R. S., Zuber, P., LaCelle, M., Marahiel, M. A., Reid, R., Khosla, C., and Walsh, C. T. (1996) A new enzyme superfamily - the phosphopantetheinyl transferases. *Chem. Biol.* 3, 923–936.
- (18) Fichtlscherer, F., Wellein, C., Mittag, M., and Schweizer, E. (2000) A novel function of yeast fatty acid synthase. Subunit alpha is capable of self-pantetheinylation. *Eur. J. Biochem.* 267, 2666–2671.
- (19) Leibundgut, M., Jenni, S., Frick, C., and Ban, N. (2007) Structural basis for substrate delivery by acyl carrier protein in the yeast fatty acid synthase. *Science* 316, 288–290.
- (20) Lomakin, I. B., Xiong, Y., and Steitz, T. A. (2007) The crystal structure of yeast fatty acid synthase, a cellular machine with eight active sites working together. *Cell* 129, 319–332.
- (21) Chalut, C., Botella, L., de Sousa-D'Auria, C., Houssin, C., and Guilhot, C. (2006) The nonredundant roles of two 4'-phosphopantetheinyl transferases in vital processes of *Mycobacteria*. *Proc. Natl. Acad. Sci. U. S. A.* 103, 8511–8516.
- (22) Leblanc, C., Prudhomme, T., Tabouret, G., Ray, A., Burbaud, S., Cabantous, S., Mourey, L., Guilhot, C., and Chalut, C. (2012) 4'-Phosphopantetheinyl transferase PptT, a new drug target required for *Mycobacterium tuberculosis* growth and persistence in vivo. *PLoS Pathog.* 8, e1003097.
- (23) Stuible, H. P., Meier, S., and Schweizer, E. (1997) Identification, isolation and biochemical characterization of a phosphopantetheine:protein transferase that activates the two type-I fatty acid synthases of *Brevibacterium ammoniagenes*. *Eur. J. Biochem.* 248, 481–487.
- (24) Quadri, L. E., Sello, J., Keating, T. A., Weinreb, P. H., and Walsh, C. T. (1998) Identification of a *Mycobacterium tuberculosis* gene cluster encoding the biosynthetic enzymes for assembly of the virulence-conferring siderophore mycobactin. *Chem. Biol.* 5, 631–645.
- (25) Kremer, L., Nampoothiri, K. M., Lesjean, S., Dover, L. G., Graham, S., Betts, J., Brennan, P. J., Minnikin, D. E., Locht, C., and Besra, G. S. (2001) Biochemical characterization of acyl carrier protein (AcpM) and malonyl-CoA:AcpM transacylase (mtFabD), two major components of *Mycobacterium tuberculosis* fatty acid synthase II. *J. Biol. Chem.* 276, 27967–27974.
- (26) Schaeffer, M. L., Agnihotri, G., Kallender, H., Brennan, P. J., and Lonsdale, J. T. (2001) Expression, purification, and characterization of the *Mycobacterium tuberculosis* acyl carrier protein, AcpM. *Biochim. Biophys. Acta* 1532, 67–78.
- (27) Dym, O., Albeck, S., Peleg, Y., Schwarz, A., Shakkeb, Z., Burstein, Y., and Zimhony, O. (2009) Structure-function analysis of the acyl carrier protein synthase (AcpS) from *Mycobacterium tuberculosis*. *J. Mol. Biol.* 393, 937–950.
- (28) Gokulan, K., Aggarwal, A., Shipman, L., Besra, G. S., and Sacchettini, J. C. (2011) *Mycobacterium tuberculosis* acyl carrier

- protein synthase adopts two different pH-dependent structural conformations. *Acta Crystallogr., Sect. D Biol. Crystallogr.* 67, 657–669.
- (29) Vickery, C. R., Kosa, N. M., Casavant, E. P., Duan, S., Noel, J. P., and Burkart, M. D. (2014) Structure, Biochemistry, and Inhibition of Essential 4'-Phosphopantetheinyl Transferases from Two Species of Mycobacteria. *ACS Chem. Biol.* 9, 1939–1944.
- (30) Zimhony, O., Cox, J. S., Welch, J. T., Vilchez, C., and Jacobs, W. R., Jr. (2000) Pyrazinamide inhibits the eukaryotic-like fatty acid synthetase I (FASI) of *Mycobacterium tuberculosis*. *Nat. Med.* 6, 1043–1047.
- (31) Unger, T., Jacobovitch, Y., Dantes, A., Bernheim, R., and Peleg, Y. (2010) Applications of the Restriction Free (RF) cloning procedure for molecular manipulations and protein expression. *J. Struct Biol.* 172, 34–44.
- (32) Peleg, Y., and Unger, T. (2012) Resolving bottlenecks for recombinant protein expression in *E. coli*. *Methods Mol. Biol.* 800, 173–186.
- (33) Arakawa, T., Ejima, D., Tsumoto, K., Obeyama, N., Tanaka, Y., Kita, Y., and Timasheff, S. N. (2007) Suppression of protein interactions by arginine: a proposed mechanism of the arginine effects. *Biophys Chem.* 127, 1–8.
- (34) Owen, J. G., Copp, J. N., and Ackerley, D. F. (2011) Rapid and flexible biochemical assays for evaluating 4'-phosphopantetheinyl transferase activity. *Biochem. J.* 436, 709–717.
- (35) Takahashi, H., Kumagai, T., Kitani, K., Mori, M., Matoba, Y., and Sugiyama, M. (2007) Cloning and characterization of a *Streptomyces* single module type non-ribosomal peptide synthetase catalyzing a blue pigment synthesis. *J. Biol. Chem.* 282, 9073–9081.
- (36) Thompson, J. D., Higgins, D. G., and Gibson, T. J. (1994) CLUSTAL W: improving the sensitivity of progressive multiple sequence alignment through sequence weighting, position-specific gap penalties and weight matrix choice. *Nucleic Acids Res.* 22, 4673–4680.
- (37) Gouet, P., Courcelle, E., Stuart, D. I., and Metoz, F. (1999) ESPript: analysis of multiple sequence alignments in PostScript. *Bioinformatics* 15, 305–308.
- (38) Rottier, K., Faillé, A., Prudhomme, T., Leblanc, C., Chalut, C., Cabantous, S., Guilhot, C., Mourey, L., and Pedelacq, J. D. (2013) Detection of soluble co-factor dependent protein expression in vivo: application to the 4'-phosphopantetheinyl transferase PptT from *Mycobacterium tuberculosis*. *J. Struct Biol.* 183, 320–328.
- (39) Wall, L., Rodriguez, A., and Meighen, E. (1986) Intersubunit transfer of fatty acyl groups during fatty acid reduction. *J. Biol. Chem.* 261, 15981–15988.
- (40) Shi, Y., Mowery, R. A., Ashley, J., Hentz, M., Ramirez, A. J., Bilgicer, B., Slunt-Brown, H., Borchelt, D. R., and Shaw, B. F. (2012) Abnormal SDS-PAGE migration of cytosolic proteins can identify domains and mechanisms that control surfactant binding. *Protein Sci.* 21, 1197–1209.
- (41) Bunkoczi, G., Pasta, S., Joshi, A., Wu, X., Kavanagh, K. L., Smith, S., and Oppermann, U. (2007) Mechanism and substrate recognition of human holo ACP synthase. *Chem. Biol.* 14, 1243–1253.
- (42) Chirgadze, N. Y., Briggs, S. L., McAllister, K. A., Fischl, A. S., and Zhao, G. (2000) Crystal structure of *Streptococcus pneumoniae* acyl carrier protein synthase: an essential enzyme in bacterial fatty acid biosynthesis. *EMBO J.* 19, 5281–5287.
- (43) Barry, C. E., 3rd, and Blanchard, J. S. (2010) The chemical biology of new drugs in the development for tuberculosis. *Curr. Opin Chem. Biol.* 14, 456–466.
- (44) Mondino, S., Gago, G., and Gramajo, H. (2013) Transcriptional regulation of fatty acid biosynthesis in mycobacteria. *Mol. Microbiol.* 89, 372–387.
- (45) Finking, R., Solsbacher, J., Konz, D., Schobert, M., Schafer, A., Jahn, D., and Marahiel, M. A. (2002) Characterization of a new type of phosphopantetheinyl transferase for fatty acid and siderophore synthesis in *Pseudomonas aeruginosa*. *J. Biol. Chem.* 277, 50293–50302.
- (46) Foley, T. L., Young, B. S., and Burkart, M. D. (2009) Phosphopantetheinyl transferase inhibition and secondary metabolism. *FEBS J.* 276, 7134–7145.
- (47) Yasgar, A., Foley, T. L., Jadhav, A., Inglese, J., Burkart, M. D., and Simeonov, A. (2010) A strategy to discover inhibitors of *Bacillus subtilis* surfactin-type phosphopantetheinyl transferase. *Mol. Biosyst.* 6, 365–375.
- (48) Banerjee, A., Dubnau, E., Quernard, A., Balasubramanian, V., Um, K. S., Wilson, T., Collins, D., de Lisle, G., and Jacobs, W. R., Jr. (1994) inhA, a gene encoding a target for isoniazid and ethionamide in *Mycobacterium tuberculosis*. *Science* 263, 227–230.
- (49) Vilchez, C., Wang, F., Arai, M., Hazbon, M. H., Colangeli, R., Kremer, L., Weisbrod, T. R., Alland, D., Sacchettini, J. C., and Jacobs, W. R., Jr. (2006) Transfer of a point mutation in *Mycobacterium tuberculosis* inhA resolves the target of isoniazid. *Nat. Med.* 12, 1027–1029.
- (50) Wilson, R., Kumar, P., Parashar, V., Vilchez, C., Veyron-Churlet, R., Freundlich, J. S., Barnes, S. W., Walker, J. R., Szymonifka, M. J., Marchiano, E., Shenai, S., Colangeli, R., Jacobs, W. R., Jr., Neiditch, M. B., Kremer, L., and Alland, D. (2013) Antituberculosis thiophenes define a requirement for Pks13 in mycolic acid biosynthesis. *Nat. Chem. Biol.* 9, 499–506.